

PACS numbers: 07.85.Fv; 07.85.Nc
DOI: 10.1070/QE2015v045n04ABEH015595

Conception of broadband stigmatic high-resolution spectrometers for the soft X-ray range

E.A. Vishnyakov, A.N. Shatokhin, E.N. Ragozin

Abstract. **We formulate an approach to the development of stigmatic high-resolution spectral instruments for the soft X-ray range ($\lambda \leqslant 300$ Å), which is based on the combined operation of normal-incidence multilayer mirrors (including broadband aperiodic ones) and grazing-incidence reflection gratings with nonequidistant grooves (so-called VLS gratings). A concave multilayer mirror serves to produce a slightly astigmatic image of the radiation source (for instance, an entrance slit), and the diffraction grating produces a set of its dispersed stigmatic spectral images. The width of the operating spectral region is determined by the aperiodic structure of the multilayer mirror and may range up to an octave in wavelength.**

Keywords: *multilayer mirrors, VLS gratings, astigmatism, soft X-ray spectral region.*

1. Introduction

Classical grazing-incidence spectral instruments with concave diffraction gratings for a wavelength range $\lambda \sim 20-300$ Å are, as is well known, astigmatic. Because of the grazing incidence on the grating, radiation is not focused in the direction perpendicular to the plane of dispersion, and the spectral image of a point source (for instance, a point of the entrance slit) is therefore a line segment, which may be several times longer than the illuminated segment of the grating groove. This entails a lowering in the irradiance of spectral lines and the loss of information about the spatial intensity distribution of the radiation source. The use of focusing normal-incidence multilayer mirrors (MMs) in combination with diffraction gratings (DGs) whose groove spacing varies across the aperture according to a specified law permits overcoming these limitations.

In 1893, Cornu [1] realised that uniform variations in the groove spacing across the aperture of a reflection DG modified the curvature of the diffracted wavefronts and the location of the focus of the spectrum. He determined that a plane grating with the requisite systematic variation in its groove spacing, if used in a collimated incident beam, would focus the diffracted beam. At present, diffraction gratings with a groove spacing varying according to a prescribed law are referred to as varied line-space gratings (VLS gratings).

In the 1980s, Harada, Hettrick and Underwood addressed their attention to these ideas. Harada et al. [2] developed a mechanical ruling engine capable of ruling plane and concave VLS gratings with the following parameters: nominal grooves density of 300–4800 grooves mm^{-1}, minimal radius of curvature of 10 mm, maximal ruled area size of 150×100 mm and minimal VLS-grating spacing increment of 0.2 Å. Employing a concave VLS grating, Harada made an astigmatic grazing-incidence spectrograph with a flat focal field for a 5–25 nm spectral domain, which has gained wide acceptance and has come to be known as the Harada spectrograph. More recently, Harada upgraded the ruling engine to make it capable of ruling gratings with a density of up to 10^4 grooves mm^{-1} [3]. Nowadays, plane VLS gratings are also made by interference lithography techniques [4]. Hettrick [5] designed a stigmatic spectrometer for recording extrasolar objects radiating in the far VUV region. In this case, use was made of three plane grazing-incidence VLS gratings for the ranges 70–90 Å, 140–380 Å and 280–760 Å, which were illuminated by the converging beam from a Wolter–Schwarzschild Type II telescope. Subsequently, Hettrick et al. developed several astigmatic laboratory VLS-grating spectrometers possessing high and ultrahigh resolution [6]. Today, VLS gratings enjoy wide use in diverse specialised spectrometers intended for investigating the emission spectra of laser-produced and fast electric-discharge plasmas, in synchrotron radiation channels, free-electron lasers, in the analysis of biological samples, etc. One of the main virtues of VLS-grating-based instruments is the possibility to design a spectrometer with a flat focal field and normal radiation incidence on a detector.

Our intention is to combine the advantages offered by VLS gratings with the capabilities of focusing MMs, including broadband aperiodic MMs. It is possible to make mirrors with a different width of the spectral reflectivity profile based on aperiodic multilayer structures. This line of research has received international recognition and is steadily advancing, primarily as applied to the multilayer optics for synchrotron radiation and diverse laser-plasma experiments with femtosecond multiterawatt lasers [7].

2. Schematic of a stigmatic spectrometer

The progress of soft X-ray multilayer optics has led to the development of high-efficiency imaging normal-incidence MMs for a wavelength range $\lambda = 66-400$ Å. In the near-normal incidence of radiation, these mirrors are capable of forming a

E.A. Vishnyakov P.N. Lebedev Physics Institute, Russian Academy of Sciences, Leninsky prosp. 53, 119991 Moscow, Russia; e-mail: juk301@mail.ru;
A.N. Shatokhin, E.N. Ragozin Moscow Institute of Physics and Technology (State University), Institutskii per. 9, 141700 Dolgoprudnyi, Moscow region, Russia; P.N. Lebedev Physics Institute, Russian Academy of Sciences, Leninsky prosp. 53, 119991 Moscow, Russia; e-mail: enragozin@gmail.com

Received 23 June 2014
Kvantovaya Elektronika **45** (4) 371–376 (2015)
Translated by E.N. Ragozin

virtually homocentric beam of rays from a point source and direct it onto a DG. However, a reflection DG with equidistant grooves, when placed in a converging beam, will itself introduce a significant astigmatism (Fig. 1), i.e. a spatial divergence of the spectral (horizontal) and vertical foci*. The vertical focus lies on the circumference centred at point O of radius L_1, which is equal to the length of line segment OA – the distance of the beam focus from the grating centre. For inner diffraction orders ($m > 0$, $\psi > \varphi$), the spectral focus (point B) lies outside of this circumference (OB > OA); for outer orders ($m < 0$, $\psi < \varphi$), it lies inside the circumference. The distance of the spectral focus of mth order from the grating centre is defined by the formula

$$L_m = L_1 \frac{\sin^2\psi}{\sin^2\varphi},$$

and the smaller the angle of grazing incidence on the DG, the stronger the astigmatism.

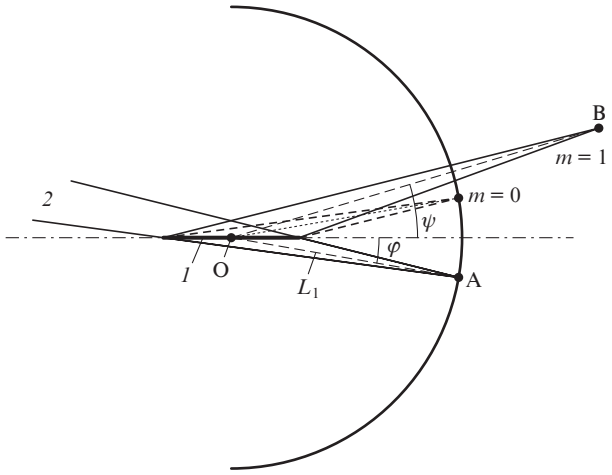

Figure 1. Astigmatism of a plane DG illuminated by a converging homocentric beam at grazing incidence:
(*1*) plane DG with equidistant grooves; (*2*) homocentric beam; (A) focus of the homocentric beam; (B) spectral focus of the beam reflected from the plane grating with equidistant grooves.

Hettrick et al. [5] specified the law which the groove spacing of a plane VLS grating must obey to bring into coincidence the spectral and vertical foci at a specified wavelength in the incidence of a converging homocentric beam on the grating (Fig. 2):

$$\frac{1}{p(w)} = d(w) = \frac{m\lambda_1}{\cos\varphi(w) - \cos\psi(w)}, \qquad (1)$$

where w is the coordinate in the grating aperture measured from the grating centre in the direction perpendicular to the grooves; $p(w)$ is the groove density at the point with coordinate w; $d(w)$ is the groove spacing; m is the working diffraction order; and $\varphi(w)$ and $\psi(w)$ are the grazing angles of incidence and diffraction. In this case, the rays that lie in the principal plane of the grating and emanate from an arbitrary point w will diffract in the requisite direction to produce the point image of a point source at a wavelength λ_1.

*The focus of the beam rays lying in the dispersion plane is termed spectral (horizontal). The focus of the rays lying in the perpendicular beam section is said to be vertical. These foci may not coincide (astigmatism).

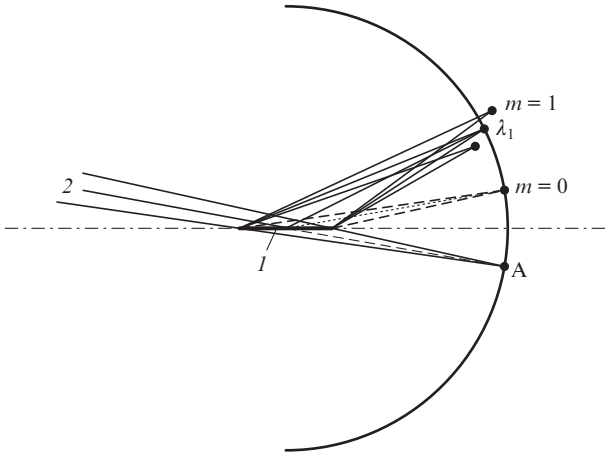

Figure 2. Compensation of astigmatism at one wavelength for a plane VLS grating:
(*1*) plane DG with nonequidistant grooves; (*2*) homocentric beam; (A) focus of the homocentric beam.

In the present work we are dealing with the possibility of designing a stigmatic spectrograph which possesses a high resolution and a strong dispersion, typical of grazing-incidence configurations, and simultaneously a relatively high luminosity as well as a large field of view due to the use of a VLS grating in combination with a concave normal-incidence MM, which directs a nearly homocentric converging beam onto the grating. The multilayer mirror structure may be periodic as well as aperiodic (Fig. 3). In the former case, the spectral reflectivity profile is bell-shaped and relatively narrow; in the latter case, this profile may be imparted, for instance, a trapezoidal shape (a constant reflectivity in a specified wavelength interval) [8]. The operating spectral range of this spectrometer (Fig. 4) will be determined by the MM reflectivity spectrum. The first calculations (outlined in our work) will be made for an aperiodic Mo/Si multilayer mirror with a uniform reflectivity (~15%–20%) in the 125–250 Å

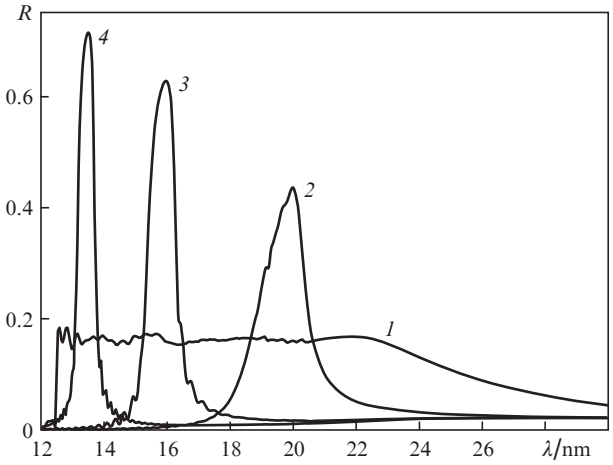

Figure 3. Reflection coefficient of an aperiodic MM optimised for maximum uniform reflectivity at normal incidence in a 12.5–25 nm range (*1*). Shown for comparison are the reflection coefficients of periodic MMs optimised for maximum reflectivity at λ = (*2*) 20, (*3*) 16 and (*4*) 13.5 nm.

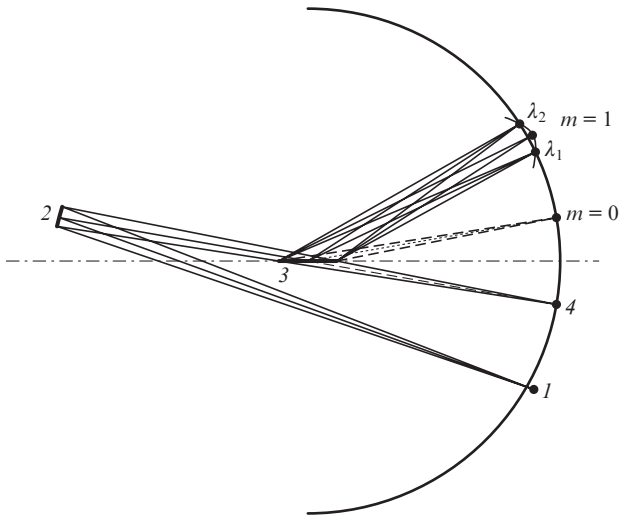

Figure 4. Optical configuration of a spectrometer with astigmatism compensation at two wavelengths:
(*1*) radiation source; (*2*) concave aperiodic MM; (*3*) plane VLS grating; (*4*) vertical focus of the converging beam.

range. The aperiodic MMs of this type were synthesised in V.V. Kondratenko's laboratory at the National Technical University 'Kharkov Polytechnic Institute' (KhPI) and were repeatedly used in experiments (see, for instance, Refs [7, 9]).

In the configuration under discussion, the spherical MM is mounted at a small angle to the central ray and introduces a small astigmatism into the converging beam. Let L_1 and L_2 denote the distances of the grating centre from the vertical and horizontal foci of the converging weakly astigmatic beam, with $L_2 < L_1$ and $L_1 - L_2 \ll L_1$. The explicit dependence of the requisite groove density on w is of the form

$$p(w) = \frac{1}{m\lambda_1}\left\{\cos\left[\operatorname{arccot}\left(\cot\varphi_0 - \frac{w}{L_1\sin\varphi_0}\right)\right] - \cos\left[\operatorname{arccot}\left(\cot\psi_0 - \frac{w}{L_2\sin\psi_0}\right)\right]\right\}, \quad (2)$$

with the notation $\varphi_0 = \varphi(w = 0)$ and $\psi_0 = \psi(w = 0)$. This variation of the grating groove density cancels astigmatism at only one wavelength λ_1.

We note that parameters φ_0, ψ_0, λ_1, m and $p_0 = p(0)$ are related by the equation for the diffraction of the central ray

$$\cos\varphi_0 - \cos\psi_0 = mp_0\lambda_1. \quad (3)$$

In this equation, any four parameters of the set φ_0, ψ_0, λ_1, m and p_0 are free, while the fifth is uniquely defined by the remaining ones. For instance, by fixing m and λ_1 we still obtain two free parameters. Traditionally, these parameters are φ_0 and p_0, while the angle ψ_0 of central ray diffraction is found from Eqn (3). Then, it is possible to obtain the expression for the groove density $p(w)$ from expression (2).

By using the remaining degrees of freedom, it is possible to demand the fulfilment of the stigmatism condition at a second wavelength λ_2. After this, there remains only one degree of freedom. It is possible to set the angle of incidence φ_0 on the grating, and then ψ_0 is determined from the equation

$$\cos\psi_0 = \cos\varphi_0 - \left[\left(\frac{L_1}{L_2} - 1\right)\frac{\lambda_1}{\lambda_2}\sin^2\varphi_0\right]^{1/2}, \quad (4)$$

and p_0 is determined from Eqn (3). Conversely, the value of p_0 may be set, and then

$$\varphi_0 = \arcsin\left(\frac{mp_0\sqrt{\lambda_1\lambda_2}}{\sqrt{L_1/L_2 - 1}}\right). \quad (5)$$

Therefore, by setting one of the two parameters, φ_0 or p_0, we find the other one from Eqns (4) or (5); after this, we determine the angle of diffraction ψ_0 from Eqn (3). We substitute all these parameters in Eqn (2) to obtain the groove density variation law $p(w)$. One can see from expressions (4) and (5) that the elimination of the instrument's astigmatism at the second wavelength turns out to be possible due to precisely the existence of a weak astigmatism ($L_2 \neq L_1$) of the beam that the MM directs onto the DG.

By limiting the number of degrees of freedom in the configuration, we manage to bring into coincidence the horizontal and vertical foci at two wavelengths, λ_1 and λ_2, i.e. the horizontal and vertical focal surfaces intersect at the two selected wavelengths. Calculations show that this surface has no kinks, and hence the condition of unrigourous stigmatism is fulfilled for a whole wavelength range. The unrigourous stigmatism (the residual astigmatism) signifies that the spectrograph constructs two-dimensional spectral images of an object with a good spatial resolution along and across the dispersion direction.

3. Spectral images of a point source

The absence of astigmatism at two wavelengths for the selected law $p(w)$ signifies that thin radiation beams with wavelengths λ_1 and λ_2 which lie in the principal (dispersion) plane do not experience aberrations for any grating width. Radiation beams of other wavelengths and beams with a finite vertical convergence angle, of course, do experience aberrations. That is why the quality of spectral images must be verified by numerical ray tracing; in the end, the optimal grating width and groove length will be determined by a trade-off between luminosity and resolution.

As discussed above, the weakly astigmatic converging beam is formed by a concave spherical MM placed nearly normally to the incident radiation beam. Given below are the simulations of imaging spectrometer characteristics performed by numerical ray tracing using the SHADOWVUI extension of X-Ray Oriented Programs (XOP) Software Package v.2.3 (available for free download on the ESRF website [10]). By way of example, we took the following configuration parameters: an operating spectral range of 120–300 Å, a radius of curvature of the mirror $R_c = 1$ m, and a grating centre–MM distance of 0.5 m. The wavelengths λ_1 and λ_2 are selected in such a way as to minimise the maximal geometric defocusing of the image of a point source caused by departure of the horizontal focal curve from the vertical one in the 120–300 Å interval. In this case, the images of a point source at the wavelengths λ_1 and λ_2 are minimal in size. In all configuration versions considered below, as it turned out, the minimal geometric defocusing condition is fulfilled when $\lambda_1 \approx 144$ Å and $\lambda_2 \approx 272$ Å. The indicated parameter set uniquely defines the law $p(w) = p_0 + p_1w + p_2w^2 + p_3w^3$ of groove density variation across the grating aperture. Table 1 shows the parameters of six spectrometer versions; the value of φ_0 was specified in the first two versions and the value of p_0 in versions three through six. The grating coefficients p_0–p_3 for all six spectrometer versions are collected in Table 2.

Table 1. Main characteristics of grazing-incidence spectrometers with a MM (R_c = 1 m), a grating centre–MM distance of 0.5 m and the entrance slit placed on the Rowland circle of the MM.

Version number	φ_0/°	p_0/mm^{-1}	α/°	Length of a 120–300 Å spectrum on the detector/mm	$\langle d\lambda/dl\rangle$/Å mm^{-1}	$\delta\lambda_{144}$/Å	Ω/sr
1	5	775	5	36	5.0	0.057	3.5×10^{-4}
2	10	915	3	32	5.6	0.067	7.0×10^{-4}
3	3.86	600	5	37.5	4.8	0.064	2.7×10^{-4}
4	7.75	1200	5	43	4.2	0.049	5.4×10^{-4}
5	6.49	600	3	28	6.4	0.075	4.5×10^{-4}
6	13.07	1200	3	35	5.1	0.063	9.1×10^{-4}

Notes: α denotes the angle of incidence of the central ray on the mirror; $\langle d\lambda/dl\rangle$ is the average plate scale in the 120–300 Å interval; $\delta\lambda_{144}$ is the spectral interval corresponding to a detector cell width of 13 μm for a wavelength of 144 Å; and Ω is the input (acceptance) solid angle.

Table 2. Parameters p_i of groove density variation law for the diffraction gratings from Table 1.

Version number	p_0/mm^{-1}	p_1/mm^{-2}	p_2/mm^{-3}	p_3/mm^{-4}
1	775	2.97	8.45×10^{-3}	2.00×10^{-5}
2	915.23	3.51	9.83×10^{-3}	2.39×10^{-5}
3	600	2.31	6.63×10^{-3}	1.67×10^{-5}
4	1200	4.53	12.6×10^{-3}	3.03×10^{-5}
5	600	2.33	6.74×10^{-3}	1.71×10^{-5}
6	1200	4.52	12.3×10^{-3}	2.83×10^{-5}

In particular, in version 1 the groove density varies in a range of 706–855 mm^{-1} across a grating of width 50 mm (w varies in the limits ±25 mm) (Fig. 5). In this case, the indicated spectral interval corresponds to a 36-mm long area on the detector, and the average plate scale is equal to 5 Å mm^{-1}. The working region on the grating measures 50×20 mm, which corresponds to the spectrometer solid acceptance angle of 3.5×10^{-4} sr. Figure 6 shows the 144-Å image of a point source lying in the principal plane as well as the intensity distribution in the direction of dispersion (the histogram at the right) and in the vertical direction (the histogram at the top). One can see that the astigmatic image blur amounts to ~10 μm at the base and the blur in the direction of dispersion, also at the base, amounts to about 6 μm. Therefore, the size of the image of a point source corresponds to the cell size (13 μm) of modern CCD detectors. The plate scale at λ_1 = 144 Å is equal to 4.35 Å mm^{-1}, and the cell size corresponds to a resolution of 5.66×10^{-2} Å and a resolving power of 2.5×10^3. The image of a point source at a wavelength λ_2 = 272 μm is similar to the image in Fig. 6.

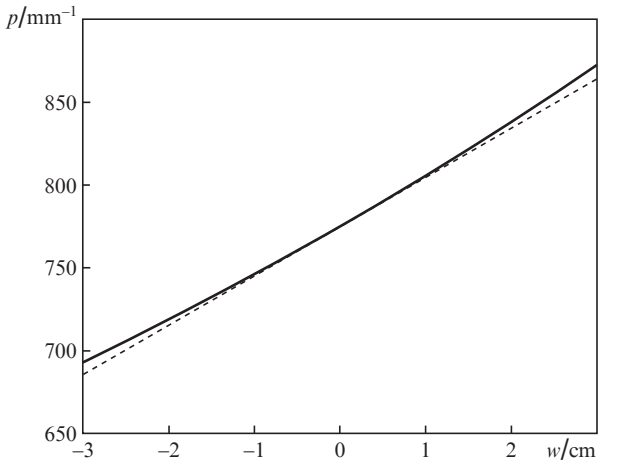

Figure 5. Dependence $p(w)$ for spectrometer version 1 (with an angle of grazing incidence of 5°). Shown for comparison is a linear approximation of this dependence (the dashed line).

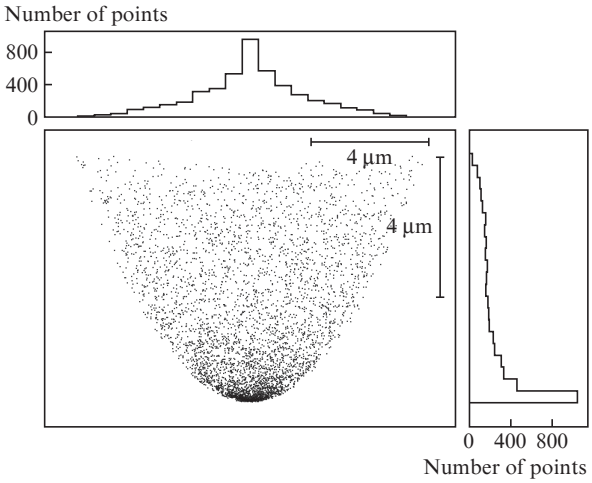

Figure 6. λ_1 = 144 Å image of a point source located in the principal plane, as well as intensity distributions in the direction of dispersion (the histogram at the right) and in the vertical direction (the histogram at the top). The simulation was performed by numerical ray tracing.

Figure 7 shows the image of a point source at a wavelength λ = 210 Å, which is characterised by the maximum geometric defocusing in the 120–300 Å operating spectral range. One can see that the image blur in both directions is equal to 15–20 μm at the base. The λ = 210 Å image of a point source spaced at ±1 cm from the principal plane is shown in Fig. 8. It is evident that there occurred a hardly noticeable impairment of the image. This signifies that the admissible height of the entrance slit is no less than 2 cm. The image quality at the edges of the range (120 and 300 Å) is the same.

Interestingly, this configuration, which is intended for operation as a spectrometer with an immobile grating, may be employed as a monochromator with immobile entrance and output slits and a rotatable grating. The resolving power will be equal to at least ~10^3 throughout the spectral range, without decreasing the solid acceptance angle.

If the acceptance angle is to be increased, it is expedient to select an angle of grazing incidence on the grating φ_0 = 10° (version 2), which leads to a different law $p(w)$. To prevent the grating groove density from becoming undesirably high, the angle of incidence on the mirror is to be lowered, for instance,

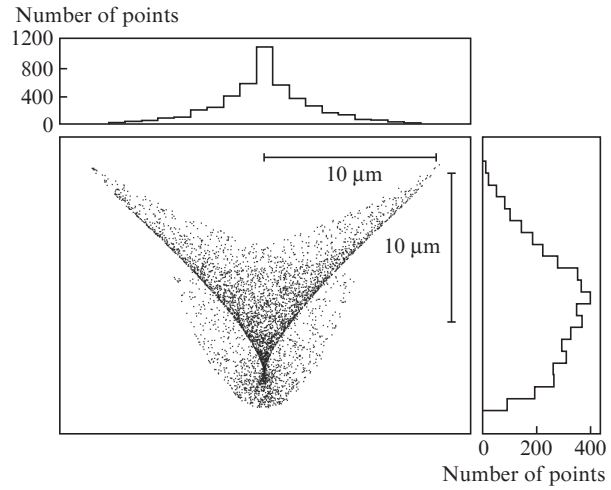

Figure 7. λ = 210 Å image located in the principal plane (the case of maximal defocusing).

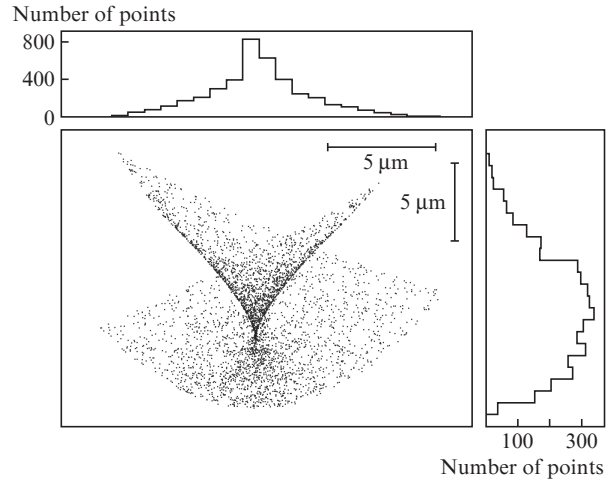

Figure 8. λ = 210 Å image of a point source spaced at ±1 cm from the principal plane (the case of maximum defocusing).

to 3°. Selecting these parameters gives $p_0 = 915$ mm^{-1}. In this spectrometer version, the acceptance angle is two times larger, the length of the working spectrum on the detector is somewhat shorter (32 mm instead of 36 mm), and the size of the image of a point source in the direction of dispersion is one-and-a-half times smaller (~6–7 μm vs. ~10 μm at the point of maximum defocusing at λ = 210 Å). However, in this case the practical resolving power is defined by the detector cell size (13 μm) and is somewhat lower. An advantage of this spectrometer version (with a large angle φ_0 and a small angle α) is its two times higher luminosity.

4. Special features of using a special purpose VLS grating

The configuration discussed above, which constructs stigmatic spectral images of the spectrometer entrance slit on the plane sensitive detector surface, corresponds to the formulation of experiment whereby the radiation source is either located directly in the plane of the entrance spectrometer slit or is imaged onto it with retention of spatial resolution. The former case corresponds to a version of a dispersive X-ray microscope [11, 12] and is not always possible or necessary; the latter may be realised using a normal-incidence MM or, for instance, a grazing-incidence ellipsoid mirror. (In a longer-wavelength domain (λ = 520.6 Å, the 4→3 transition of C VI ions) Aglitskii et al. [13] took advantage of a concave spherical mirror with an iridium reflective coating.) In experiments, however, it is not infrequent that the source (for instance, the laser plasma of a solid or cluster target) may be positioned at a short distance (say, 35 mm) from the entrance slit and in doing this the spatial resolution in the 'vertical' direction (i.e., along the slit) is to be retained. This problem is solved without changing the VLS grating. Below we explain the way of going over to the configuration whereby the vertical focus of the source spaced at 35 mm from the entrance slit is located on the detector as before.

For specified φ_0, λ_1 and λ_2, the VLS-grating parameters (p_1, p_2, p_3) are completely defined by the distances L_1 and L_2. It is also implied that the mirror does not introduce aberrations other than a minor astigmatism ($L_1 - L_2 \ll L_1$). Without changing the magnitude of the mirror astigmatism $L_1 - L_2$ and varying the angle of incidence α on the MM, it is possible to vertically focus the source points located at a short preassigned distance from the entrance slit, and in doing so retain the spectral focusing of the slit image on the detector. For this formulation of the experiment, it is possible to employ the same VLS gratings as before. To attain this in spectrometer version 6, for instance, the angle of incidence on the mirror should be increased from 3° to 8°. Simulations performed by numerical ray tracing suggest that the spectral images of an extended (in the horizontal direction) source located at a distance of 35 mm in front of the entrance source do not exceed the size of one detector cell.

5. Broadband MMs for the $\lambda < 125$ Å range

The instruments developed on the basis of a broadband aperiodic MM and a VLS grating also hold promise for operation at shorter wavelengths ($\lambda < 125$ Å).

Theoretical simulations suggest that different pairs of materials, judging by their optical constants, might serve the purpose of making aperiodic MMs with a broad reflection band under the L edge of Si, in the $\lambda < 125$ Å domain [9]. However, these simulations do not take into consideration the technological aspect of the problem and, which is extremely important, the stability of the structures relative to the formation of transition layers. Without going into the technological aspect of the problem, we note that one of the best candidates is the La/B_4C pair of materials, whose optical constants permit designing a structure with a constant reflectivity of ~4.2% (neglecting the formation of transition layers) in a spectral range of 6.6–11 nm (Fig. 9). The lower bound of the optimisation domain is determined by the position of the K absorption edge of boron (λ = 65.9 Å), while the upper bound may be arbitrarily selected. In this case, shifting the long-wavelength bound of the optimisation domain from 110 to 88 Å is not attended with an appreciable gain in reflectivity of the aperiodic MM. But shifting the short-wavelength bound of the optimisation domain to 88 Å has the result that the constant reflectivity of the aperiodic MM rises to 7.2% in the 88–110 Å domain.

The recent progress in making La/B_4C multilayer structures achieved by the team of Salashchenko [14] gives hope for the synthesis of aperiodic MMs on thier basis for spectroscopy in the 66–110 Å range. In Ref. [14], it has been possible

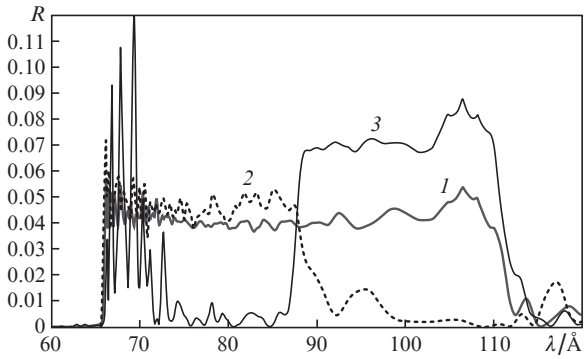

Figure 9. Calculated reflectivity of aperiodic La/B_4C multilayer structures optimised for maximum uniform reflectivity in the spectral ranges (*1*) 66–110 Å, (*2*) 66–88 Å and (*3*) 88–110 Å.

to largely suppress the formation of transition layers in the La/B_4C structure due to the use of extremely thin (~3 Å) carbon barrier layers and thereby attain a record value of reflectivity (58.6%) for a periodic structure at $\lambda = 66.6$ Å for a near-normal radiation incidence.

Furthermore, broadband Sb/B_4C mirrors for the 100–120 Å range with an integral reflection coefficient of ~1 Å have recently been synthesised in the KhPI [15]. Sb/B_4C structures exhibit a high stability, and MMs based on such structures can provide peak reflectivities of 19%–28% in a spectral range of 66–85 Å [16].

6. Conclusions

The combined use of a concave spherical aperiodic MM mounted almost normally to the incident radiation and a plane VLS grating at a grazing incidence permits making a high-resolution stigmatic spectrometer with a broad (more than an octave in wavelength) operating spectral range of 120–300 Å. In this case, the solid acceptance angle amounts to $(3–9)\times10^{-4}$ sr and the vertical field of view to about 2 cm. A special feature of the formulated approach consists in that the stigmatism condition [the coincidence of the vertical and spectral (horizontal) foci] is simultaneously achieved for two preassigned wavelengths (in this case, at 144 and 272 Å), which was substantiated and realised for the first time in this configuration. The progress in the development of broadband aperiodic MMs for $\lambda < 125$ Å will subsequently make it possible to extend the range of application of stigmatic VLS spectrometers.

Acknowledgements. This work was supported by the Russian Science Foundation (Grant No. 14-12-00506).

References

1. Cornu M.A. *Comptes Rendus Acad. Sci.*, **117**, 1032 (1893).
2. Harada T., Kita T. *Appl. Opt.*, **19** (23), 3987 (1980).
3. Kita T., Harada T. *Appl. Opt.*, **31** (10), 1399 (1992).
4. Amemiya K., Kitajima Y. *J. Synchrotron Rad.*, **3**, 282 (1996).
5. Hettrick M.C., Bowyer S., Malina R.F., Martin C., Mrowka S. *Appl. Opt.*, **24** (12), 1737 (1985).
6. Hettrick M.C., Underwood J.H., Batson P.J., Eckart M.J. *Appl. Opt.*, **27** (2), 200 (1988).
7. Kando M., Pirozhkov A.S., Kawase K., et al. *Phys. Rev. Lett.*, **103** (23), 235003 (2009).
8. Kolachevskii N.N., Pirozhkov A.S., Ragozin E.N. *Kvantovaya Elektron.*, **30** (5), 428 (2000) [*Quantum Electron.*, **30** (5), 428 (2000)].
9. Vishnyakov E.A., Kamenets F.F., Kondratenko V.V., Luginin M.S., Panchenko A.V., Pershin Yu.P., Pirozhkov A.S., Ragozin E.N. *Kvantovaya Elektron.*, **42** (2), 143 (2012) [*Quantum Electron.*, **42** (2), 143 (2012)].
10. http://www.esrf.eu/Instrumentation/software/data-analysis/xop2.3.
11. Ilyukhin A.A., Peregudov G.V., Ragozin E.N. *Pis'ma Zh. Tekh. Fiz.*, **47** (4), 1341 (1976).
12. Feldman U., Doschek G.A., Prinz D.K., Nagel D.J. *J. Appl. Phys.*, **47** (4), 1341 (1976).
13. Aglitskii E.V., Boiko V.A., Zakharov S.M., Sklizkov G.V. Preprint of the P.N. Lebedev Physics Inst., No. 143 (Moscow, 1970).
14. Chkhalo N.I., Künstner S., Polkovnikov V.N., Salashchenko N.N., Schäfers F., Starikov S.D. *Appl. Phys. Lett.*, **102**, 011602 (2013).
15. Vishnyakov E.A., Voronov D.L., Gullikson E.M., Kondratenko V.V., Kopylets I.A., Luginin M.S., Pirozhkov A.S., Ragozin E.N., Shatokhin A.N. *Kvantovaya Elektron.*, **43** (7), 666 (2013) [*Quantum Electron.*, **43** (7), 666 (2013)].
16. Kopylets I.A., Kondratenko V.V., Zubarev E.N., Voronov D.L., Gullikson E.M., Vishnyakov E.A., Ragozin E.N. *Appl. Surf. Sci.*, **307**, 360 (2014).